

# A Time-Relative Approach for Precise Positioning with a Miniaturized L1 GPS Logger

J. Traugott, Institute of Flight System Dynamics, Technische Universität München, Germany  
G. Dell’Omo, TechnoSmArt, Rome, Italy

A.L. Vyssotski, Institute of Anatomy, University Zürich-Irchel, Switzerland

D. Odijk, Delft Institute of Earth Observation and Space Systems, Delft University of Technology, the Netherlands

G. Sachs, Institute of Flight System Dynamics, Technische Universität München, Germany

## BIOGRAPHY

Johannes Traugott received his diploma degree in Mechanical Engineering with focus on Aerospace Technology at Technische Universität München in 2004. He then joined the Institute of Flight System Dynamics as a research assistant. His interests lie in satellite navigation and flight path reconstruction.

Giacomo Dell’Omo has been working as a scientist on animal behavior since 1990. In 2006 he launched the company TechnoSmArt in Rome and is currently developing light-weight GPS dataloggers for tracking birds and small mammals.

Alexei Vyssotski got his degree of engineer-physicist at the faculty of Physico-Chemical Biology of Moscow Institute of Physics and Technology in 1995 and he defended his Ph.D. Thesis in Physiology in 2001. Now he is working as a researcher at the Institute of Anatomy, University of Zurich. His interests lie in the area of animal navigation and electrophysiology.

Dennis Odijk holds a PhD in Geodetic Engineering of Delft University of Technology. At present, he works as a researcher with the Delft Institute for Earth Observation and Space systems (DEOS). He is involved in several GNSS-related projects, focusing on ambiguity resolution, modeling of the ionosphere for precise positioning and indoor applications.

Gottfried Sachs is Professor of Flight Mechanics and Flight Control at Technische Universität München. One of his research activities is concerned with the application of miniaturized navigation systems to the flight dynamics of aircraft and birds.

## ABSTRACT

L1 phase measurements collected by an autonomous, miniaturized and low cost GPS logging device are the basis for the navigation approach discussed in the present paper. Forming single differences between two measurements taken by one moving receiver at two different times allows to achieve

relative precision in the low decimeter range over time intervals of up to several minutes. Neither a second, nearby base receiver nor any (static) initialization procedures are required by the method. This fact significantly reduces the complexity to be handled by the user often operating under adverse field conditions. The approach is taking advantage of canceling ambiguities instead of striving for estimating these unknown quantities every phase measurement is biased with. The constitutive navigation equations are derived elaborately and theoretic aspects of various error sources restricting possible processing intervals are discussed in this paper. A geometric error raising from an offset in the initial position is analyzed in particular. The results of a static experiment confirm the theoretic considerations. Furthermore, technical details of the utilized GPS logger are given and data collected during two flight experiments are validated and compared with different reference solutions.

## INTRODUCTION

Reducing weight, size, power consumption and complexity for the user is the primary focus of today’s mass market targeting GPS community. The present approach outlines a possibility to expand this idea to scientific applications where the principal objective is precision augmentation. This goal is striven for by postprocessing raw L1 phase observations recorded by a miniaturized, completely self contained GPS logging unit.

The proposed approach allows for the precise measurement of dynamic flight maneuvers in order to analyze the air vehicle’s motion in a flight-mechanical sense. Among other things this requires position fixes which are precise relative to the starting point of the maneuver of interest within the low decimeter range. The maneuvers themselves are limited in time to a view minutes only. High dynamics demands for raised sampling rates of at least 10 Hz. As miniaturized air vehicles and even birds are to be measured, the sensor used must operate completely autonomous and has to be both lightweight ( $\leq 100$  g) and small ( $\leq 150 \times 50 \times 20$  mm<sup>3</sup>). The weight restriction entails low power con-

sumption for a runtime of up to 50 - 70 hours just as budget limitations imply the use of low cost sensors. The latter requirements are readily met by standard single frequency GPS receiver modules as used in car navigation systems or latest generation cell phones. Some of these modules output raw data, i.e. pseudorange, carrier phase, Doppler frequency and raw signal strength or SNR values, with up to 10 Hz. Logging these raw (phase) measurements for precise postprocessing instead of sticking to the code based online navigation solution qualifies these receiver modules as appropriate sensors for the described flight measurement task. Note that the online navigation solution is restricted to sampling rates well below the rate the raw measurements are provided with. Conventional phase based processing techniques rely on the presence of data collected by a nearby ( $\leq 10$  km) base station and (mostly static) initialization patterns of the roving receiver. Both cannot be provided in the scope of the current applications: birds neither remain static nor close to a base station and miniaturized air vehicles can perform maneuvers such as loops which inevitably cause signal shadowing resulting in complete loss of lock undoing any kind of initialization. Hence an alternative way to process the L1 phase measurements with no need for a base station or an initialization phase is presented in this paper. The price to be paid for these advantages is a limitation in processing time to a view minutes. A detailed description of the theoretic concept is given as well as a practical validation by various field and flight experiments.

## THEORETICAL BACKGROUND

### The Observable: L1 Phase Ranges

The present method is based on the L1 phase range observable generated in the phase lock loop (PLL) of a GPS receiver. This measurement shall briefly be reviewed in this section: The nominal (constant) frequency  $f$  of the L1 carrier wave is 1575.42 MHz. Let  $\varphi^S(t)$  [cycles] designate the phase of the satellite emitted wave as perceived by the receiver and  $\varphi^R(t)$  [cycles] denote the phase of the (not yet Doppler compensated) receiver replica signal. With  $t$  [s] as an epoch in GPS system time reckoned from an initial epoch  $t_0 (= 0)$  when acquiring lock to the respective PRN one can state:

$$\varphi^S(t) = ft - f\frac{\rho(t)}{c} - \varphi_0^S(t) \quad \varphi_0^S(t) = -\delta^S(t)f + \varphi^S(t_0) \quad (1)$$

$$\varphi^R(t) = ft - \varphi_0^R(t) \quad \varphi_0^R(t) = -\delta^R(t)f + \varphi^R(t_0). \quad (2)$$

Here,  $\varphi_0^S$  and  $\varphi_0^R$  are the satellite and receiver initial phase biases at  $t_0$  afflicted with the respective clock errors  $\delta^S$  and  $\delta^R$  [s] ( $\delta > 0 \leftrightarrow$  clock reading ahead of GPS system time). The symbol  $\rho$  [m] is the geometric distance between satellite and receiver;  $c$  [m/s] denotes the nominal signal propagation speed in vacuum. The beat phase  $\phi^{RS}$  [cycles] is now given by

$$\begin{aligned} \phi^{RS}(t) &= \varphi^S(t) - \varphi^R(t) \\ &= -f\frac{\rho(t)}{c} - \delta^{RS}(t)f + \varphi^R(t_0) - \varphi^S(t_0) \end{aligned} \quad (3)$$

with the combined satellite and receiver clock error  $\delta^{RS} = \delta^R - \delta^S$ . Note that due to the initial distance between satel-

lite and receiver  $\rho(t_0)$ , Eq. (3) theoretically yields a large decimal number for the beat phase  $\phi^{RS}(t)$ . However when acquiring lock to the respective PRN only the fractional part of this number can be measured, the initial integer number  $N$  of cycles between satellite and receiver is unknown. Note that this ambiguity is not time dependent as long as the phase is locked continuously:  $N \neq N(t)$ . Hence, to model the numerical value actually output by the receiver, this unknown but constant integer term  $N$  has to be subtracted from the right-hand side of Eq. (3). Moreover, to obtain a value directly corresponding to a geometric range, the result is multiplied by  $-\lambda_1$  (the L1 wavelength) yielding the (pseudo) phaserange  $\Phi$  [m]:

$$\Phi(t) = \rho(t) + c\delta^{RS}(t) + \lambda_1 \underbrace{(\varphi^S(t_0) - \varphi^R(t_0) + N)}_{N'} \quad (4)$$

Neither the initial satellite nor receiver phase  $\varphi^S(t_0)$ ,  $\varphi^R(t_0)$  are known. Hence the non-integer ambiguity term  $N'$  is introduced as shown in Eq. (4) to finally rewrite for the L1 phaserange:

$$\Phi(t) = \rho(t) + c\delta^{RS}(t) + \lambda_1 N' \quad (5)$$

In literature the non-integer ambiguity term  $N'$  is frequently replaced by the integer ambiguity  $N$ . This is not precise in a strict sense but the fractional receiver and satellite phase terms only drop out and a truly integer ambiguity term is obtained when forming double differences. However, the non-integer character of the undifferenced phase observations does play an important role for procedures such as precise point positioning (Gao 2006). It is important to keep in mind that the phase observable changes in the same sense as the C/A code pseudorange (negative doppler) but is significantly less noisy.

### Basic Concept

The principal idea of the present approach is the fact that the ambiguity  $N'$  is time-invariant, provided lock of phase. Hence, differencing phase observations to the same satellite  $S$  across two epochs  $t_b$  and  $t_i$  allows for canceling  $N'$ :

$${}^{bi}\nabla\Phi = \Phi_i - \Phi_b = {}^{bi}\nabla\rho + c{}^{bi}\nabla\delta^R + \lambda_1 \cancel{{}^{bi}\nabla N'} \quad (6)$$

with  $\nabla$  denoting single temporal differences. The right hand side subscript  $i$  shall be a short equivalent for the time argument ( $t_i$ ) during the following derivations. Note that the satellite clock error  $\nabla\delta^S$  is neglected in Eq. (6).

The shown way to cancel ambiguities is the background for a diversity of applications. In tightly coupled GPS/INS systems time differenced double differences (so called triple differences across two receivers, two satellites and two epochs) can support the dynamics estimation for attitude computation (Farrell 2001). In a similar context, also carrier phases directly differenced between subsequent epochs can be used instead of the noisier delta-range measurements to improve velocity and attitude information without the need for a base station (Wendel et al. 2003). Triple differences can also be used for carrier phase cycle slip detection (Kim et al. 2002).

Further, precise baseline computation between a base and a roving receiver provided that there are at least 7 satellites (if only phase data are used) in view is possible with triple differences (Graas et al. 1995). Time-differences used in a stand-alone GPS application are used to process static data for gun-laying applications (Ulmer et al. 1995). This approach, enhanced by a loop misclosure procedure, can be applied to static measurements from civil receivers since selective availability has been switched off (Balard et al. 2006).

Using time differences for processing kinematic data is an unconventional approach emerged from the need for a high quality but low effort navigation solution. The navigation equations are derived in the following.

### Navigation Equations

Assume the position  $\mathbf{x}^R$  of the receiver to be known at a (base) epoch  $t_b$ . Then one can write for the base vector pointing from the position at the base epoch to the position at the epoch of interest  $t_i$

$$\mathbf{b}^{bi} = \mathbf{x}^R(t_i) - \mathbf{x}^R(t_b) \quad (7)$$

Fig. 1 illustrates the geometry of the problem. Besides the

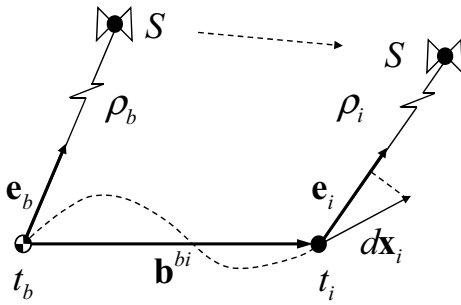


Figure 1. Basic principle of time differences.

position, the receiver clock error with respect to GPS system time has to be determined, yielding the combined position and time (PT) variable:

$$\xi = [\mathbf{x}^R, c\delta^R]^T \quad (8)$$

Here the clock error is scaled to range by multiplication with the signal propagation speed for convenience. Now one can set up the enhanced base vector

$$\beta^{bi} = \xi_i - \xi_b \quad (9)$$

In order to determine  $\beta^{bi}$ , time differences  $^{bi}\nabla\Phi$  between two phase observations at  $t_b$  and  $t_i$  as introduced in Eq. (6) are used. For precise navigation, the phase range, Eq. (5), has to be enhanced by models for signal delays caused by ionospheric and tropospheric refraction,  $\hat{I}$  and  $\hat{T}$ :

$$\hat{\Phi}_i = \hat{\rho}_i + c\delta_i^R + \lambda_1 N' + \hat{T}_i - \hat{I}_i \quad (10)$$

Here the symbol  $\hat{\cdot}$  is introduced to distinguish modeled from measured values denoted by  $\tilde{\cdot}$ . The unknown satellite clock

error can not be modeled and is therefore omitted in Eq. (10). The geometric range is calculated by

$$\hat{\rho}_i = \|\mathbf{x}_i^S - \mathbf{x}_i^R\| \quad (11)$$

where  $\mathbf{x}_i^S$  is the satellite position at the time of signal emission corresponding to the epoch  $t_i$ . This position is extracted from the Ephemeris data of the respective satellite. Now the time differenced phase observations can be rewritten as

$$\begin{aligned} ^{bi}\nabla\hat{\Phi} &= ^{bi}\nabla\hat{\rho} + c^{bi}\nabla\delta^R - ^{bi}\nabla\hat{I} + ^{bi}\nabla\hat{T} \\ &= f(\xi_i, \xi_b) \end{aligned} \quad (12)$$

Note that in a strict sense  $\nabla\hat{\Phi}$  is not a function of  $\beta$  but of both the PT solution at the current epoch and the (known) base epoch. In order to solve for  $\xi_i$ , at least four measurements are required:

$$^{bi}\nabla\tilde{\Phi} \stackrel{!}{=} ^{bi}\nabla\hat{\Phi} \quad (13)$$

with

$$\begin{aligned} ^{bi}\nabla\tilde{\Phi} &= \begin{bmatrix} ^{bi}\nabla\tilde{\Phi}^1 & ^{bi}\nabla\tilde{\Phi}^2 & \dots & ^{bi}\nabla\tilde{\Phi}^m \end{bmatrix}^T \\ ^{bi}\nabla\hat{\Phi} &= \begin{bmatrix} ^{bi}\nabla\hat{\Phi}^1 & ^{bi}\nabla\hat{\Phi}^2 & \dots & ^{bi}\nabla\hat{\Phi}^m \end{bmatrix}^T \end{aligned} \quad m \geq 4$$

Just as for standard single point processing, this (overdetermined) set of equations is solved by the nonlinear least squares method. For that purpose, the right hand side of Eq. (13) has to be linearized:

$$^{bi}\nabla\hat{\Phi}(\xi_i, \xi_b) = ^{bi}\nabla\hat{\Phi}(\xi_{i,0}, \xi_b) + \mathbf{H}_{\xi_{i,0}} \Delta\xi_i \quad (14)$$

The linearization point  $\xi_{i,0}$  is either the result of the last iteration cycle of the current epoch or the final result of the previous epoch. The Jacobian writes elaborately as

$$\mathbf{H}_{\xi_{i,0}} = \left. \frac{d^{bi}\nabla\hat{\Phi}}{d\xi_i} \right|_{\xi_{i,0}} = \begin{bmatrix} \frac{\partial ^{bi}\nabla\hat{\Phi}^1}{\partial x_i^R} & \frac{\partial ^{bi}\nabla\hat{\Phi}^1}{\partial y_i^R} & \frac{\partial ^{bi}\nabla\hat{\Phi}^1}{\partial z_i^R} & \frac{\partial ^{bi}\nabla\hat{\Phi}^1}{\partial (c\delta_i^R)} \\ \frac{\partial ^{bi}\nabla\hat{\Phi}^2}{\partial x_i^R} & \frac{\partial ^{bi}\nabla\hat{\Phi}^2}{\partial y_i^R} & \frac{\partial ^{bi}\nabla\hat{\Phi}^2}{\partial z_i^R} & \frac{\partial ^{bi}\nabla\hat{\Phi}^2}{\partial (c\delta_i^R)} \\ \vdots & \vdots & \vdots & \vdots \\ \frac{\partial ^{bi}\nabla\hat{\Phi}^m}{\partial x_i^R} & \frac{\partial ^{bi}\nabla\hat{\Phi}^m}{\partial y_i^R} & \frac{\partial ^{bi}\nabla\hat{\Phi}^m}{\partial z_i^R} & \frac{\partial ^{bi}\nabla\hat{\Phi}^m}{\partial (c\delta_i^R)} \end{bmatrix}_{\xi_{i,0}} \quad (15)$$

With eqs. (10) and (12) the following relationships hold

$$\begin{aligned} \frac{\partial ^{bi}\nabla\hat{\Phi}}{\partial \mathbf{x}_i^R} &\approx \frac{\partial \hat{\rho}_i}{\partial \mathbf{x}_i^R} = -\mathbf{e}_i \\ \frac{\partial ^{bi}\nabla\hat{\Phi}}{\partial (c\delta_i^R)} &= 1 \end{aligned} \quad (16)$$

where  $\mathbf{e}_i$  is the unit vector pointing from the rover position at  $t_i$  to the satellite, compare Fig. 1. Spatial variations of the atmospheric models are neglected when linearizing as these effects are compensated for by the iteration. With Eq. (16) the Jacobian rewrites to

$$\mathbf{H}_{\xi_{i,0}} = \begin{bmatrix} -\mathbf{e}_{i,0}^T & 1 \\ \vdots & \vdots \\ -\mathbf{e}_{i,0}^T & 1 \end{bmatrix} \quad (17)$$

Now one obtains with least squares for  $\Delta\xi_i$

$$\Delta\xi_i = \left( \mathbf{H}_{\xi_{i,0}}^T \mathbf{H}_{\xi_{i,0}} \right)^{-1} \mathbf{H}_{\xi_{i,0}}^T \left( {}^{bi}\nabla\tilde{\Phi} - {}^{bi}\nabla\widehat{\Phi}(\xi_{i,0}, \xi_b) \right) \quad (18)$$

and iteration

$$\xi_{i,k+1} = \xi_{i,k} + \Delta\xi_i \quad (19)$$

finally yields  $\xi_i$ . For the sake of clarity the inversion of the normal equation matrix is stated in Eq. (18). A direct solution by using e.g. Cholesky decomposition is recommended for the practical implementation. Note that even so the PT solution directly drops out of the solution process,  $\xi_i$  is precise relative to  $\xi_b$  only and its absolute accuracy depends on the one of  $\xi_b$  itself. Consequently,  $\beta^{bi}$  is the intrinsic solution of the problem. This will become even more evident in Eq. (28).

The shown solving procedure minimizes the residuals  $\epsilon^j$  between measured and modeled observations in a least squares sense:

$$\sum_{j=1}^m \epsilon^j{}^2 = \min \quad (20)$$

$$\epsilon^j = {}^{bi}\nabla\tilde{\Phi}^j - {}^{bi}\nabla\widehat{\Phi}^j \quad (21)$$

If the inevitable experimental measurement errors are uncorrelated, have a mean of zero and a constant variance, the least squares estimate of  $\Delta\xi_i$  has the minimum variance of all estimates that are linear combinations of the observations. In this sense it is the optimal solution.

### Error Analysis

As indicated in Eq. (10) the phase range model is enhanced by terms taking into account atmospheric signal propagation delays. However, these effects cannot be eliminated completely. The remaining effects  $\epsilon$  compose, together with other contributions, the non-modeled range error  $\chi$ :

$$\begin{aligned} \tilde{\Phi}_i &= \widehat{\Phi}_i + \chi_i \\ \chi_i &= -c\delta_i^S + E_i + \epsilon_i + \text{noise} \end{aligned} \quad (22)$$

This error is made up by the scaled satellite clock bias  $\delta^S$ , the satellite position offset due to uncertainties in the satellite ephemeris  $E$ , the described remaining atmospheric delays  $\epsilon$  and measurement noise. When forming time differences this yields

$$\begin{aligned} {}^{bi}\nabla\tilde{\Phi} &= {}^{bi}\nabla\widehat{\Phi} + {}^{bi}\nabla\chi \\ {}^{bi}\nabla\chi &= -{}^{bi}\nabla\delta^S + {}^{bi}\nabla E + {}^{bi}\nabla\epsilon + {}^{bi}\nabla\text{noise} \end{aligned} \quad (23)$$

Except for the noise ( $\sigma_{\nabla\text{noise}} \approx \sqrt{2}\sigma_{\text{noise}}$ ) the range error components are highly temporally correlated which allows the following ‘‘linearization’’:

$${}^{bi}\nabla\chi = \left[ -c \frac{d\delta^S}{dt} + \frac{dE}{dt} + \frac{d\epsilon}{dt} \right]_{t_b} (t_i - t_b) + \left. \frac{\partial\epsilon}{\partial\mathbf{x}^R} \right|_{t_b} \mathbf{b}^{bi} + \nabla\text{noise} \quad (24)$$

The atmospheric error stemming from spatial variations occurs in any kind of differential processing and remains small

with short baseline length. As a matter of fact, the raise of the noise level can not be avoided but is smaller by a factor of  $1/\sqrt{2}$  than when working with double differences. However, the drift terms are the bottleneck problem for the time difference approach. In order to keep this effect small, precise correction data are utilized. These data not only decrease the absolute range error but also increase its temporal correlation. Usually only little attention is paid to this fact which is key for extending the precise processing time when working with time differences. However, there is yet another error source affecting the relative precision of the solution - the bias in  $\xi_b$  from the true position and time. In order to analyze this effect, Eq. (14) is linearized in both  $\xi_{i,0}$  and the true base position and time  $\xi_{b,0}$ :

$${}^{bi}\nabla\widehat{\Phi}(\xi_i, \xi_b) = {}^{bi}\nabla\widehat{\Phi}(\xi_{i,0}, \xi_{b,0}) + \mathbf{H}_{\xi_{i,0}} \Delta\xi_i - \mathbf{H}_{\xi_{b,0}} \Delta\xi_b \quad (25)$$

with the Jacobian  $\mathbf{H}_{\xi_{i,0}}$  according to Eq. (17) and  $\Delta\xi_b = \xi_b - \xi_{b,0}$ . Referring to Eqs. (10), (12) and (17) one gets for the second Jacobian

$$\mathbf{H}_{\xi_{b,0}} = - \left. \frac{\partial {}^{bi}\nabla\widehat{\Phi}(\xi_i, \xi_b)}{\partial \xi_b} \right|_{\xi_{b,0}} = \begin{bmatrix} -\mathbf{e}_{b,0}^{1T} & 1 \\ \vdots & \vdots \\ -\mathbf{e}_{b,0}^{mT} & 1 \end{bmatrix} \quad (26)$$

The minus sign is used for convenience only in order to obtain analogy between  $\mathbf{H}_{\xi_{i,0}}$  and  $\mathbf{H}_{\xi_{b,0}}$ . Fig. 1 illustrates the geometry of the unit vectors. The matrices  $\mathbf{H}_{\xi_{b,0}}$  and  $\mathbf{H}_{\xi_{i,0}}$  are closely related which allows again to linearize:

$$\mathbf{H}_{\xi_{b,0}} = \mathbf{H}_{\xi_{i,0}} + \dot{\mathbf{H}}_{\xi_i} (t_b - t_i) = \mathbf{H}_{\xi_{i,0}} + \begin{bmatrix} -\dot{\mathbf{e}}_{i,0}^{1T} & 0 \\ \vdots & \vdots \\ -\dot{\mathbf{e}}_{i,0}^{mT} & 0 \end{bmatrix} (t_b - t_i) \quad (27)$$

Note that Eq. (27) only takes into account the changes due to the time elapsed between base and rover epoch not due to the motion of the receiver. The former does have an significant impact on the unit vectors due to the motion of the satellites themselves whereas the latter is neglected due to the far distance between receiver and satellites. Inserting Eq. (27) in Eq. (25) yields

$$\begin{aligned} {}^{bi}\nabla\widehat{\Phi}(\xi_i, \xi_b) &= {}^{bi}\nabla\widehat{\Phi}(\xi_{i,0}, \xi_{b,0}) + \\ &+ \mathbf{H}_{\xi_{i,0}} \underbrace{(\Delta\xi_i - \Delta\xi_b)}_{\Delta\beta^{bi}} + \underbrace{\dot{\mathbf{H}}_{\xi_i} (t_i - t_b)}_{{}^{bi}\nabla\chi_{\text{geo}}} \Delta\xi_b \end{aligned} \quad (28)$$

The last term of Eq. (28) is unknown and can, in analogy to  $\nabla\chi$ , Eq. (23), be interpreted as a geometric range error caused by variable satellite geometry:

$$\begin{aligned} {}^{bi}\nabla\chi_{\text{geo}}^j &= -\dot{\mathbf{e}}_i^{jT} \Delta\xi_b (t_i - t_b) \\ {}^{bi}\nabla\chi_{\text{geo}} &= \left[ {}^{bi}\nabla\chi_{\text{geo}}^1, \dots, {}^{bi}\nabla\chi_{\text{geo}}^m \right]^T \end{aligned} \quad (29)$$

Just as the non-modeled range error  $\nabla\chi$ , the geometric range error causes an error in the relative navigation solution. Fig. 2 aims to illustrate this effect: If the position at  $t_b$  is afflicted by an offset  $\Delta\mathbf{x}_b$ , the vector  $\mathbf{b}^{bi}$  is first of all translated by

$\Delta \mathbf{x}_b$  as well. This translation causes a shift of  $\mathbf{x}_i$  by  $\Delta \mathbf{x}_b$  which is no error as relative precision is yet maintained. However, just as every other range error, also  $\nabla \chi_{\text{geo}}$  causes a distortion of  $\mathbf{b}^{bi}$ , indicated by  $\Delta \mathbf{b}^{bi}$  in the figure. This does degrade relative precision. It is interesting to note that the

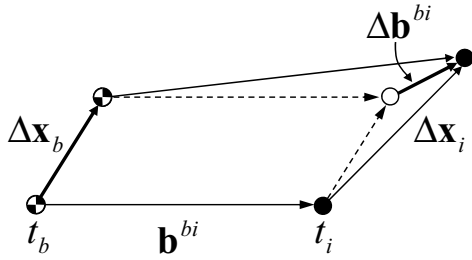


**Figure 2.** Impact of a bias in the initial epoch's position on relative precision.

variation of the satellite geometry over time has virtually no impact on the relative solution if the initial position and time  $\xi_b$  is known exactly,  $\Delta \xi_b = 0$ , no matter how long time intervals are processed.

In order to estimate the impact of the various range errors on  $\beta^{bi}$ , Eq. (23) is enhanced to

$${}^{bi}\nabla \tilde{\Phi}^j = {}^{bi}\nabla \hat{\Phi}^j + \underbrace{{}^{bi}\nabla \chi^j + {}^{bi}\nabla \chi_{\text{geo}}^j}_{{}^{bi}\nabla \chi_{\text{total}}^j} \quad (30)$$

With Eqs. (24) and (29) it can be seen that the total range error is a superposition of different random processes. Each of them has a different degree of temporal autocorrelation. For instance the change of the error caused by unprecise ephemeris is much slower than the change of the measurement noise. As only short time intervals  $t_i - t_b$  are processed, the slowly changing error contributions can be considered as systematic but unknown biases in the measurements. In other terms, the individual range errors  ${}^{bi}\nabla \chi_{\text{total}}^j$  can be assumed to be non-ergodic random processes with constant and equal variance and statistic distribution but a different, unknown expectation which is growing with time for each measurement. This fact significantly complicates the estimation of the error in  $\beta^{bi}$ . In the scope of this paper, the quality of the solution is validated via comparison with reference solutions. In addition, a simplistic estimation of the error propagation is provided by referring to the concept of Dilution Of Precision (DOP) as known from standard single point processing: Ignoring all systematic errors in the measurements for the lack of better knowledge, a rough estimation of the covariance matrix of the least squares solution is obtained by

$$\mathbf{C}_\beta = \sigma_{\nabla \tilde{\Phi}}^2 \mathbf{D}; \quad \mathbf{D} = \left( \mathbf{H}_{\xi_{i,0}}^T \mathbf{H}_{\xi_{i,0}} \right)^{-1} \quad (31)$$

For the number of measurements exceeding the number of unknowns,  $m \gg n = 4$ , the variance of the measurements is estimated from the residuals by

$$\sigma_{\nabla \tilde{\Phi}}^2 \approx \frac{\sum_{j=1}^m \epsilon_j^2}{m-4} \quad (32)$$

The DOP value referring to position accuracy is defined by

$$\text{PDOP} = \sqrt{\sum_{k=1}^3 D_{kk}} \quad (33)$$

By comparing coefficients an estimate for position quality is obtained by

$$\sqrt{\sum_{k=1}^3 C_{\beta, kk}} = \sigma_{\nabla \tilde{\Phi}} \cdot \text{PDOP} \quad (34)$$

Note that the Jacobian when working with time differences as indicated in Eq. (17) coincides with the one used when processing single points. Hence the numerical DOP values characterizing the quality of a single point solution also hold for the time difference solution.

## IMPLEMENTATION

The algorithm chosen to transform the derived navigation equations into a tool for processing real world measurement data is illustrated in Fig. 3. At the beginning of the trajectory

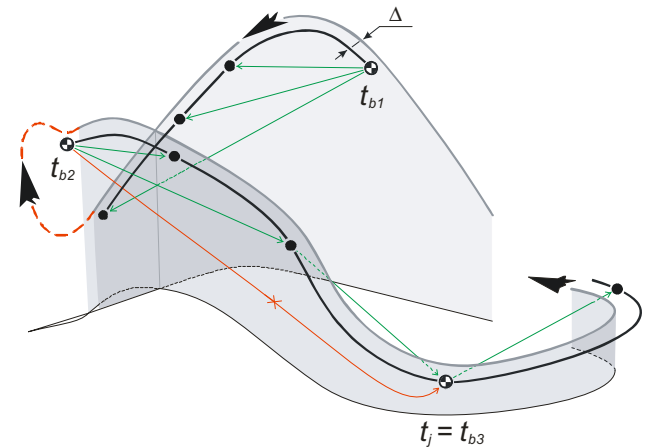


**Figure 3.** Realization of the time difference approach for processing kinematic data.

section to be analyzed, a starting point at the base epoch  $t_{b1}$  is determined via code based single point processing. The position of this point is accurate only to within a few meters and therefore offset from the true track (grey line) by  $\Delta$ . All subsequent epochs,  $t_i$  are processed using time differences between  $t_i$  and  $t_{b1}$  as long as at least 4 common satellites are available. The resulting track indicated by the black line is precise relative to the base epoch. If maneuvers causing loss-of-lock on too many satellites are performed, indicated here by the dashed red line, processing has to be aborted. Right after suchlike maneuvers, a new base position (and time) at  $t_{b2}$  can be imported from the single point solution. No re-initialization pattern has to be performed by the rover but processing can directly be continued relative to the new base. Such an event will inevitably cause a gap in the resulting trajectory. In the example case the solution fails again between the base epoch  $t_{b2}$  and the current time  $t_j$ . However, during this time there are enough common healthy satellites observed at  $t_{j-1}$  and  $t_j$  to calculate the baseline between these two points, referred to as “delta

epoch solution” from now on. A base epoch handover preventing a gap in the solution can be realized and processing is hereupon continued relative to  $t_{b3}$ .

The delta epoch solution not only serves for realizing base handovers. As this solution is calculated over very short time intervals, all range errors except for measurement noise virtually vanish, compare Eq. (24). Hence the residual level, Eq. (20), of such a solution is very low - if there are no outliers. In reverse, this property permits outlier and cycle slip detection. The latter is particularly important as cycle slips are discontinuities in the phase measurements caused by a temporary loss of lock in the receiver’s carrier tracking loop. As phase lock is a prerequisite for canceling ambiguities, compare Eq. (6), cycle slip detection is important when working with time differences. An algorithm based on these facts is currently under development.

As discussed in the above, also non-outlying, healthy measurements are afflicted by errors  $\nabla\chi_{total}$ . When working with the present approach, these errors are growing with increasing processing time spans. For attenuating the error drift different measures are taken when implementing the navigation equations. With Eq. (29) one can see that the error  ${}^{bi}\nabla\chi_{geo}$  stemming from a bias in the base solution becomes maximum if  $\Delta\xi_b$  is collinear with  $\hat{e}_i$ . According to (Ulmer et al. 1995)  $\|\dot{\hat{e}}_i\|$  does not exceed 0.00019 /s. For a processing interval of 200 s and a base position bias of 4 m the resulting range error would be 15 cm in this worst case scenario. Hence it is important to apply the range corrections used for time differential processing to attenuate error drift also when calculating the base position via code based single point processing for absolute error limitation. Tropospheric signal delays are compensated for by the UNB3 model given in (Collins et al. 1996). Ionospheric propagation delays (advances when working with phase observations) are accounted for by a thin layer model as indicated in the standard literature, e.g. (Hofmann-Wellenhof et al. 2001). Here, the total electron count (TEC) is computed from ionospheric correction maps provided free of charge by the Crustal Dynamics Data Information System in the IONEX format ([www.cddis.gsfc.nasa.gov](http://www.cddis.gsfc.nasa.gov)). Ephemeris error reduction is realized using final ephemeris products published online by the International GNSS Service (IGS, <http://igsceb.jpl.nasa.gov>) or directly by the Center of Orbit Determination in Europe (CODE). Attenuating the range error resulting from the satellite clock frequency offset, which integrates to the satellite clock error, is achieved by the use of 30 s sampled clock correction data published by (AIUB 2007). These high precise data are often used themselves as a reference to assess the quality of lower sampled clock products (Montenbruck et al. 2005). As the clock error is growing faster than the ephemeris error, these corrections are particularly important when working with time differences. More details about the effect of the described correction models on the time difference solution is given by (Traugott et al. 2008).

## PRACTICAL VALIDATION

### Static Experiment

The results of a static experiment are discussed in order to demonstrate the precision achievable by the time difference approach under very good conditions. Moreover, the effect of the geometric error stemming from an offset in the initial base position is analyzed. The test was performed on June 19, 2006 on a sports field in the north of Munich with scattered buildings nearby (48° 16’ 52.3’’ N; 11° 40’ 30.2’’ E). The used low cost receiver is a u-Blox TIM-LP single frequency module integrated in an evaluation kit provided by the manufacturer. Zero baseline tests show the standard deviation of the phase measurements of the receiver to be as low as 0.87 mm (Odijk et al. 2007). For processing, ionospheric correction maps (igs0190.06i), precise ephemeris (COD13584.EPH) and clock corrections (COD13584.CLK) are used. A time interval of 5 min is processed, which is significantly longer than the typical intervals to be analyzed for flight measurements. The bold red line of the upper plot of Fig. 4 shows the error drift during this time interval, i.e. the offset of the static relative solution from zero. Good PDOP vales of about 2.1, see lower plot, limit the error to below 3 dm. Besides the error, the estimate of the error is illustrated by the upper plot of Fig. 4: The lowest, dashed green line is the root mean square of the phase range residuals, the light blue line right above is the estimate of the standard deviation of the measurements, compare Eq. (32). Scaling with PDOP yields the 3D position error estimate as given by Eq. (34). Considering the simplifications made for calculating this estimate indicated by the bold, dotted, grey line, it matches the actual error well. However, one has to be aware that the quality of the error estimate depends on the number of used satellite and will be meaningless for the case of only four used satellites,  $m = n = 4$ . The impact of a bias

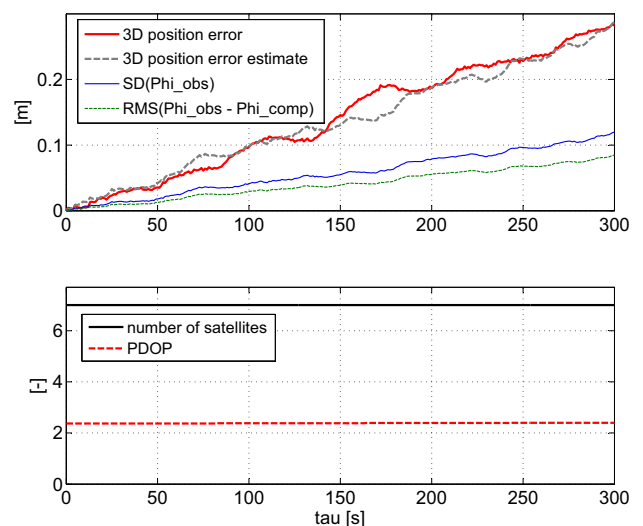
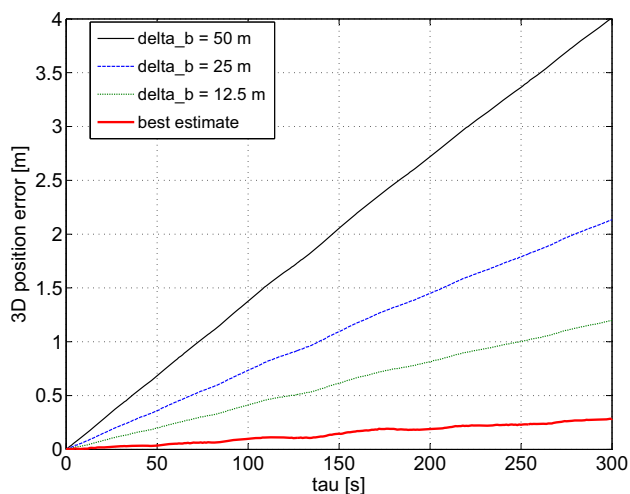


Figure 4. Static test: 3D error with quality assessment.

in the base position was discussed theoretically by Eqs. (25) through (29) and illustrated by Fig. 2. This effect is validated by adding an offset vector  $\Delta\mathbf{x}_b$  with random direction but defined length to the best estimate of the initial solution

as used above. The results are shown by Fig. 5: One can clearly see a (linear) relationship between the offset in the base position and the growing drift in the time difference solution. These results coincide well with Eq. (29) and underline the need for a good estimate of the base position and time solution. However, the results of this static test also



**Figure 5.** Static test: impact of a bias in the base position  $\Delta x_b$  on relative precision.

show that the accuracy of the time difference solution obtained when applying all mentioned corrections stays in the low decimeter (or even centimeter) range depending on the time spans to be analyzed.

### Dynamic Flight Experiments

**Hardware.** The tests described in the remainder were performed using the modified miniaturized GPS datalogger “GiPSy” from TechnoSmArt, Rome, Italy, depicted in Fig. 6. The

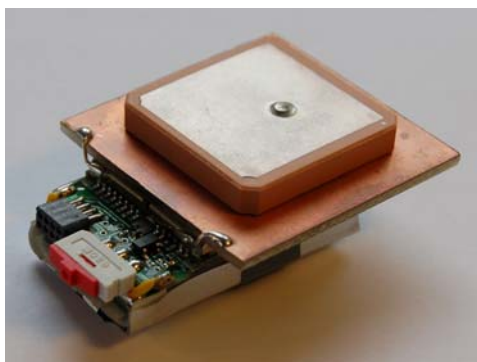


**Figure 6.** Miniaturized GPS datalogger “GiPSy” (www.techno-smart.eu) with  $25 \times 25 \text{ mm}^2$  patch antenna attached.

modifications include replacement of the standard GPS module LEA-4H with the module LEA-4T (www.u-blox.com), capable to provide raw GPS data, and exploiting signals from a  $25 \times 25 \times 4 \text{ mm}^3$  passive patch antenna placed on  $35 \times 35 \text{ mm}^2$  ground plate. Non processed raw data with a sampling rate of up to 10 Hz suitable for off-line analysis can be logged within the 8 MB internal flash memory

(approximately 40 min of recording at 10 Hz). The quality of the raw data is expected to be comparable to those of the TIM-LP receiver used for the static test. All data can be downloaded to the PC via USB using a dedicated software. An inverted connector cable also allows the direct communication with the GPS module via other programs such as u-Blox u-Center and the totally free setting of all the module’s parameters. The volume of GiPSy is as low as  $44 \times 21 \times 4 \text{ mm}^3$  at a weight of 4.25 g only without battery. Adding the patch antenna (14.15 g) and a 320 mAh 3.7 V lithium-polymeric battery (7.1 g) increased weight of the construction up to 25.5 g. The power consumption of GiPSy is approximately 40 mA. The available logging memory is extended by connecting an external serial datalogger. The schematics of this logger is similar to the digital part of the Neurologger, described in (Vyssotski et al. 2006). The logger utilizes Secure Digital (SD) memory card with the capacity up to 2 GB as data storage media. For the present experiments a 1 GB memory card was used. The volume of the serial data logger is  $50 \times 36 \times 5 \text{ mm}^3$ , its weight is 6 g and its power consumption is 6.7 mA. 1 GB of memory is sufficient to store 10 Hz raw GPS data during 5.3 days approximately.

**Flight Test with Glider Plane.** IDAFLIEG, the umbrella organization of the German academic aviation associations, arranges an annual meeting in order to analyze the flight characteristics and aerodynamic parameters of latest generation high performance glider planes. In this context the precise measurement of flight maneuvers of the tested candidate planes is required in conjunction with high fidelity airdata. For this purpose, the candidate is accompanied by the reference glider DG 300/17 operated by the German Aerospace Center (DLR). This glider is equipped with high end measurement equipment from the Technische Universität Carolo-Wilhelmina zu Braunschweig; a dual frequency Novatel OEMV receiver, precise air pressure measurement devices and a Litef inertial measurement unit are provided in conjunction with a Novatel DL-V3 (P)DGPS ground station. A photo of the flight test scenario is given by Fig. 7. The maneuvers of interest for the investigations are mostly



**Figure 7.** Glider test: test environment at IDAFLIEG summer meeting 2008, Aalen-Elchingen, Germany. Reference plane DG 300/17 (to the left) with candidate plane Venus 2cxa.

limited to short time intervals of approximately 2 min. Their analysis requires, among other things, the precise trajectory of both reference and candidate plane, with respect to a defined starting point. The time difference approach is proposed as a simple, straight forward option to provide this information. In order to firstly evaluate this possibility, the GPS logger GiPSy was placed on the instrument panel of the reference plane during a flight on August 21, 2008, starting from the airfield Aalen-Elchingen, Germany. Due to the mostly steady flight of the glider, the data quality was expected to be very good. However, frequent radio communication is identified as a possible reason for phase lock problems occurring simultaneously on all channels during wide ranges of the logged data. This problem was not observed in the data recorded by a second, identical receiver mounted in the candidate plane farther away from the radio. Hence the problem is likely to be solved by altering the position of the logger during future tests. For evaluation purposes, an unspoiled 3 min interval while towing the glider to the final flight level is chosen. Fig. 8 shows the corresponding vertical profile as obtained by processing the 10 Hz data via time differences. As for the static test, iono-

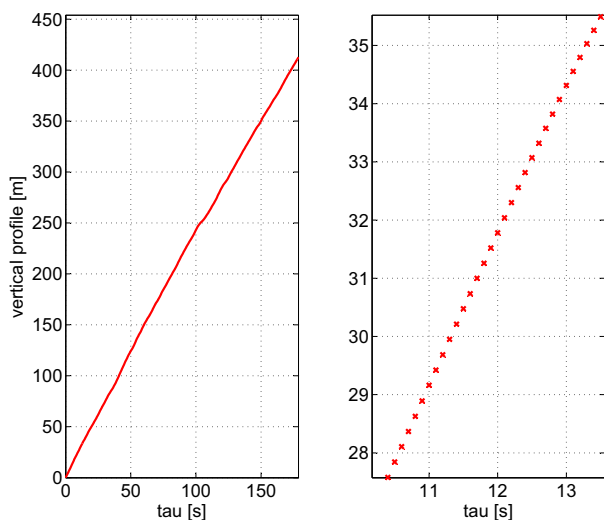


**Figure 8.** Glider test: 10 Hz sampled vertical profile of a 3 min flight section; total interval (to the left) and zoomed section.

spheric correction maps, precise ephemeris and 30 s sampled clock corrections were utilized. The estimated quality of the solution is illustrated by Fig. 9. 9 satellites yielding a PDOP of approximately 2.0 are tracked from which none is affected by a loss-of-lock event according to the corresponding indicator flag provided by the LEA-4T module. The resulting phase range residual level is indicated by the lowest, green line depicted in the upper plot of the figure. An estimate of the standard deviation of the measurements is given by the light blue line right above, compare Eq. (33). Following Eq. (34), the 3D position error is estimated to stay below 15 cm, dashed, grey line. Considering the very low residual level and the high number of used satellites, the reliability of this estimate is comparable to the static test described in the above. In order to validate the time differ-

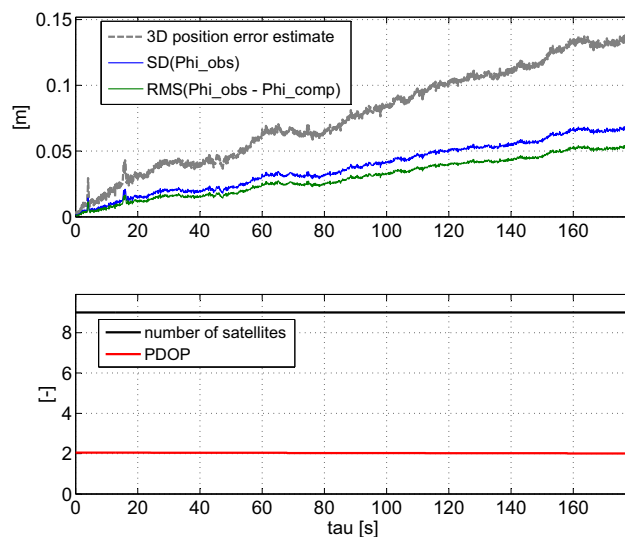


**Figure 9.** Glider test: quality analysis of the time difference solution.

ence results, an integrated GNSS/INS solution is addressed. This solution evaluates the reference INS and GNSS data from the DG 300/17 with the TriPos software package of the Institute of Flight Guidance of the Technische Universität Braunschweig. It is a highly flexible research software built on object orientated techniques. It can be configured flexibly to various setups including free combinations of filters, aiding techniques, filter models and filter types. This software is used to process different setups of the recorded flight test data. All processing is carried out in real-time configurations and with the filters mentioned. More details concerning the method can be found in (Becker et al. 2007). Due to time constraints, only a preliminary TriPos solution directly calculated on the test site right after the flight experiments was available in the scope of this paper. The 3D deviation between the results found by the time difference method and the INS/GNSS solution is indicated by Fig. 10, bold red line. In addition, the components of this deviation in cartesian WGS-84 coordinates are plotted. As the latter approach provides absolute accuracy, the position offset of the two solutions at the initial epoch  $\tau = 0$  s (i.e. at  $t_b$ ) is eliminated and only the relative deviation of the two results with respect to  $t_b$  is considered. With a maximum deviation of 38 cm this comparison confirms the quality of the results found by utilizing time differences of phase observations collected by low cost receivers.

**Flight Test with Acrobatic Plane** The results of a further flight test measured with the GPS logger “GiPSy” and processed via time differences shall be discussed in the remaining section. The flight was performed by the acrobatic plane Mü30 “Schlacro” developed and built by the academic aviation association AKAFLEG of TU München. The receiver was mounted on the outer left wing tip of the aircraft, as illustrated by Fig. 11. The 10 Hz phase data collected during a S-sequence maneuver flown close to the airfield Fürstentfeldbruck, Germany, on August 15, 2008, is analyzed. The 2D trajectory and the vertical profile of

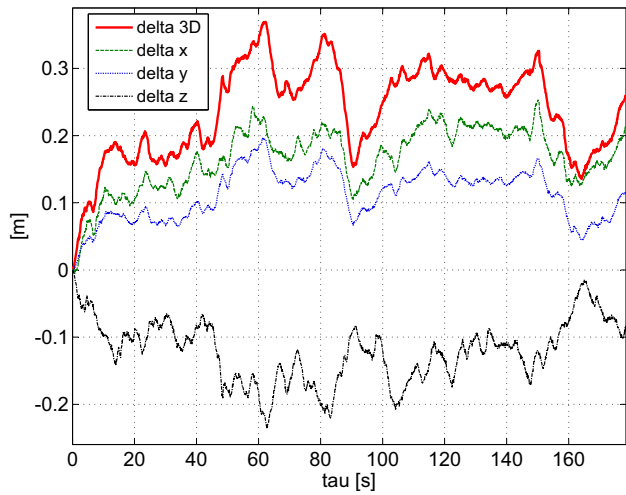


**Figure 10.** Glider test: comparison of the time difference method with a tightly coupled INS/GPS solution (courtesy of the Institut für Flugführung, Technische Universität Braunschweig).

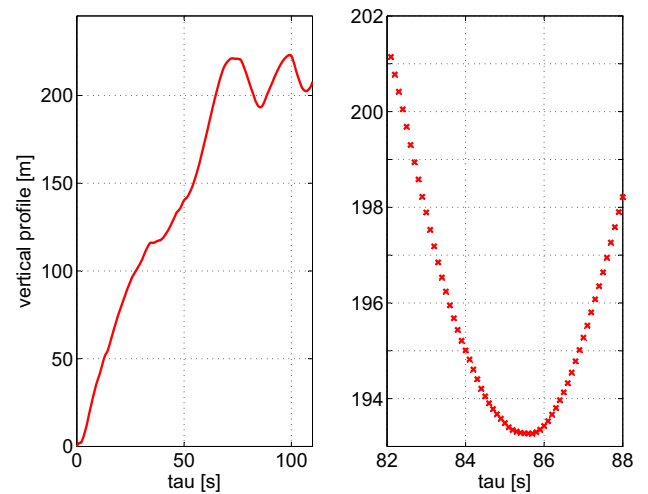


**Figure 11.** Mü30 flight test: Aircraft Mü30 “Schlacro” with GPS logger “GiPSy” mounted on left wing tip.

the maneuver is given by Fig. 12. When processing, precise ephemeris (COD14794.EPH), high rate clock solutions (COD14794.CLK) and ionospheric correction maps (igs1360.08i) are used. The quality of the collected phase measurements is good. No loss of phase lock is indicated by the receiver generated LLI flags for the 7 used PRN, compare Fig. 13 during the maneuver. The corresponding root mean square of the C/N0 values yields 48.1 dBHz. As a consequence, the residual level and the estimate of the measurement standard deviation dropping out from the least squares solver are very low, see light green and blue lines in the upper plot of Fig. 14. However, likely due to the bank angle occurring during the maneuver, the satellite geometry is worse compared to the glider test and results in (still good) PDOP values of up to 4.4, lower plot of the figure. These values are combined to the 3D error estimate, Eq. (34), indicated by the bold grey line of the upper plot of Fig. 14. The precision is estimated to be better than 17 cm. For val-



(a) 2D trajectory. (1) Start of precise relative processing; (2) end of precise relative processing.



(b) Vertical profile relative to the starting point (1) of the maneuver. Total time history (to the left) and zoomed section.

**Figure 12.** Mü30 flight test: flight trajectory during S-sequence maneuver.

idation purposes, a second receiver (u-Blox TIM-LP) was mounted close to the airfield serving as a base station for RTK processing and static initialization was provided. The fixed solution is computed in a differential (RTK) mode using the data of the base receiver. The double-differenced phase and code data of both receivers are processed using inhouse Kalman filter software of the Department of Earth Observation & Space Systems of Delft University of Technology. In this Kalman filter the (float) L1 ambiguities are kept constant but no constraints are imposed to the dynamics of the rover coordinates. The software automatically detects for cycle slips and outliers in the data and in case a cycle slip is identified the ambiguity state vector is adapted for this. For this flight test, using data of 8 satellites, it turned out that after about 3 min the float ambiguity solution had converged sufficiently such that the integer values could be estimated by means of the LAMBDA method (Teunissen 1994). After checking whether these integer ambiguities would pass the Ratio Test with fixed failure rate (Verhagen and Teunis-

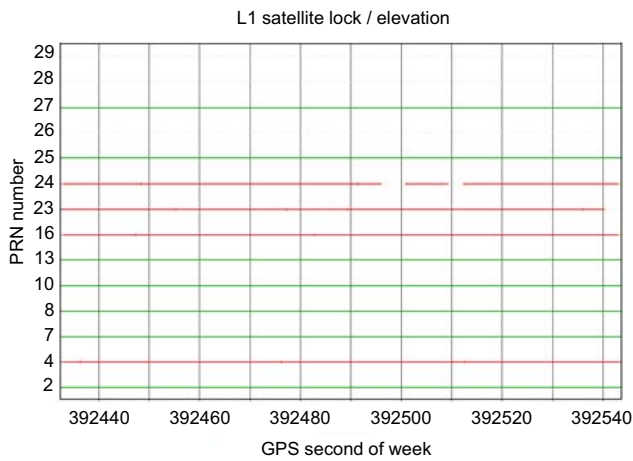


**Figure 13.** Mü30 flight test: PRN state - vertical bars indicate loss of lock as reported by the receiver's LLI flag. PRN 4, 16, 23 and 24 (red) are excluded from processing due to insufficient data quality. The remaining, used PRN are all above 30 deg elevation (green).

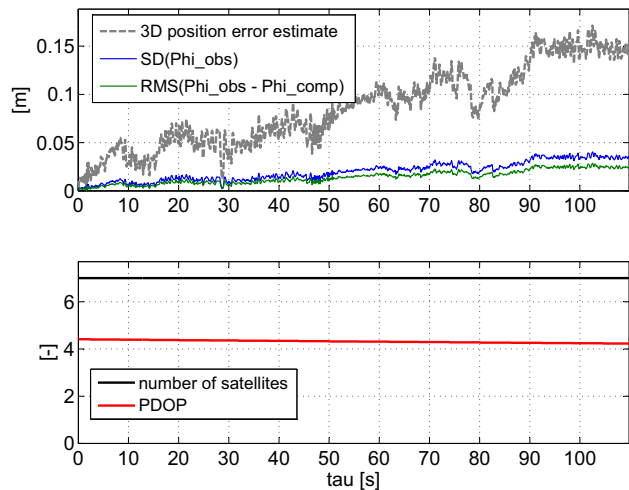


**Figure 14.** Mü30 flight test: quality analysis of the time difference solution.

sen 2006), the ambiguity-fixed solution for the rover position was computed. One cycle slip was detected 21 s after the beginning of the maneuver on PRN 4 (which was excluded for time difference processing). It is well worth to note that aside from serving as a validation of the time difference method, the RTK solution also demonstrates successful ambiguity resolution when processing data of truly low cost receivers collected in highly dynamic applications. The deviation of the obtained results from the time difference solution are shown by Fig. 15. The relative error components in local tangent coordinates do not exhibit a special trend to the hight direction and the absolute value of the 3D relative offset stays below 13 cm (again, the initial offset has been eliminated). This result confirms the high precision achievable by time differences.

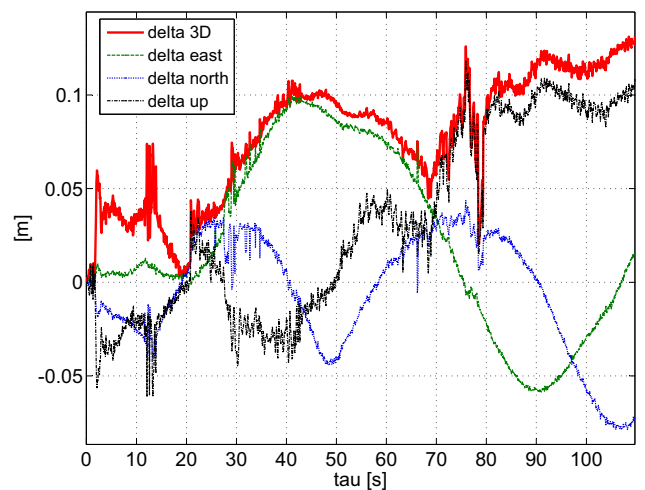


**Figure 15.** Mü30 flight test: comparison of the time difference method with a RTK solution generated by DEOS of TU Delft.

## CONCLUSIONS AND OUTLOOK

Carrier phase time differences are used in a diversity of applications and recently also gain importance in safety critical applications such as receiver autonomous integrity monitoring for aviation applications (Walter et al. 2008). A method to utilize the fact of canceling ambiguities as a stand-alone possibility to precisely process kinematic measurements over time spans of several minutes has been developed for flight measurement applications and was presented within this paper. The navigation equations underlying this approach were derived and theoretical aspects of various error sources were reflected including an estimation of their impact on the final base vector precision. The practical validation of static data gathered under favorable conditions confirmed that the temporal correlation of the remaining range errors is high. This allowed for processing time spans of up to 5 min with relative aberrations below 30 cm. Moreover, the test showed that the derived error estimate principally is a suitable means to assess the quality of the navigation solution. The impact of position biases of the base epoch was also demonstrated with the static data. Such offsets cause an additional “geometric” range error significantly distorting the baseline when exceeding 5 to 10 m. Applying the correction data used to attenuate the error drift also when calculating the initial position via code based single point processing is a suitable means to overcome this problem. Dynamic flight test results performed with a completely self-contained GPS logging device featuring a mass-market L1 single frequency GPS module were presented. The device offers the possibility to save raw measurements with sampling rates of up to 10 Hz at a weight of 25.5 g only. In conjunction with its small size, this device allows to collect raw data also in very difficult field conditions, e.g. precise bird tracking. Data gathered during a test flight with a glider plane underlined the capability of the time difference method to achieve relative precision in the low decimeter range basing on data from the small logging device. Comparison with an integrated INS/GNSS differen-

tial solution confirmed this statement as maximum deviation between both solutions did not exceed 38 cm during a 3 min processing interval. The analysis of data collected during a 110 s lasting dynamic maneuver performed by an acrobatic propeller plane further pointed out the potential of the approach. The relative deviation from a fixed ambiguity RTK reference solution stayed below 13 cm during the whole maneuver. These results can possibly be further improved by introducing a weighting factor based either on satellite elevation or SNR values in the least squares solving procedure. Moreover, algorithms taking into account measurement error cross-correlations and systematic biases can possibly also advance the results. Using the relative solution calculated between subsequent epochs for outlier and cycle slip detection was briefly discussed but is yet to be further developed for advancing the time difference method - a method which is both unconventional and easy to apply in the field: For a user who is well aware of the pitfalls of raw phase data processing, neither a second, nearby base station along with (static) initialization procedures nor high quality receiver technology is required to achieve a truly phase based, stand-alone navigation solution precise to the low decimeter range.

#### ACKNOWLEDGEMENTS

The authors would like to acknowledge Oliver Montenbruck, DLR, who strongly supported the development of the processing approach presented in this paper. Further, we would like to acknowledge the Institute of Flight Guidance of TU Braunschweig, namely Falk Pätzold and Ulf Bestmann, for having provided the INS/GNSS solution for the glider flight tests. These test would not have been possible without the straightforward cooperation offered by IDAFLIEG, which we highly appreciate. Finally we would like to acknowledge AKAFLIEG of TU München for realizing the flight experiments with the aircraft Mü30 "Schlacro".

#### REFERENCES

- Balard, N., R. Santerre, M. Cocard and S. Bourgon (2006). Single GPS receiver time-relative positioning with loop misclosure corrections. *GPS Solutions*, Vol. 10, No. 1, pp. 56-62.
- Becker, M., U. Bestmann, A. Sasse, M. Steen and P. Hecker (2007). In Flight Estimation of Gyro and Accelerometer Scale Factors for Tactical and MEMS IMUs. *Proc. of ION 20th International Technical Meeting of the Satellite Division*, Fort Worth, TX, 25-28 September 2007, pp. 2056-2065.
- CODE - Center for Orbit Determination in Europe (2007). 30s clock solutions, Astronomisches Institut Universität Bern, <ftp://ftp.unibe.ch/aiub/CODE/yyyy/CODwwwwd.CLZ.Z>
- Collins, P.C., R. Langley and J. LaMance (1996). Limiting Factors in Tropospheric Propagation Delay Error Modelling for GPS Airborne Navigation. *Proc. of ION 52nd Annual Meeting*, Cambridge, MA, 1996.
- Farrell, J.L. (2001). Carrier phase processing without integers. *Proc. of ION 57th annual meeting/CIGTF 20th biennial guidance test symposium*, Albuquerque, NM, 11-13 June 2001, pp. 423-428.
- Gao, Y. (2006). What is precise point positioning (PPP), and what are its requirements, advantages and challenges? *InsideGNSS*, Vol. 1, No. 8, pp. 16-18.
- van Graas, F and S.-W. Lee (1995). High-accuracy differential positioning for satellite-based systems without using code-phase measurements. *Journal of the Institute of Navigation*, Vol. 42, No. 4, pp. 605-618.
- Hofmann-Wellenhof, B., H. Lichtenegger and J. Collins (2001). *Global Positioning Systems, Theory and Practice*, 5th edition, Springer, Wien, New York.
- Kim, D. and R. Langley (2002). Instantaneous real-time cycle-slip correction for quality control of GPS carrier-phase measurements. *Journal of the Institute of Navigation*, Vol. 49, No. 4, pp. 205-222.
- Montenbruck, O., E. Gill and R. Kroes (2005). Rapid orbit determination of LEO satellites using IGS clock and ephemeris products. *GPS Solutions*, Vol. 9, pp. 226-235. DOI 10.1007/s10291-005-0131-0.
- Odiijk, D., J. Traugott, G. Sachs, O. Montenbruck and C.C.J.M. Tiberius (2007). Two Approaches to Precise Kinematic GPS Positioning with miniaturized L1 Receivers. *Proc. of ION 20th International Technical Meeting of the Satellite Division*, Fort Worth, TX, 25-28 September 2007, pp. 827-838.
- Teunissen, P.J.G. (1994). A New Method for Carrier Phase Ambiguity Estimation. *Proc. of IEEE PLANS*, Las Vegas, NV, 11-12 April 1994, pp. 862-873.
- Traugott, J., D. Odiijk, O. Montenbruck and C.C.J.M. Tiberius (2008). Making a Difference with GPS. *GPS World*, Vol. 19, No. 5, pp. 48-57.
- Ulmer, K., P. Hwang, B. Disselkoe and M. Wagner (1995). Accurate azimuth from a single PLGR+GLS DoD GPS receiver using time relative positioning. *Proc. of ION GPS-95*, Palm Springs, CA, 12-15 September 1995, pp. 1733-1741.
- Verhagen, S., P.J.G. Teunissen (2006). New Global Navigation Satellite System Ambiguity Resolution Method Compared to Existing Approaches. *Journal of Guidance, Control and Dynamics*, Vol. 29, No. 4, pp. 981-991.
- Vyssotski, A.L., A.N. Serkov, P.M. Itskov, G. Dell'Omo, A.V. Latanov, D.P. Wolfer and H.-P. Lipp (2006). Miniature Neurologgers for Flying Pigeons: Multichannel EEG and Action and Field Potentials in Combination with GPS Recording. *Journal of Neurophysiology*, Vol. 95, pp. 1263-1273.

Walter, T., J. Blanch, P. Enge, B. Pervan and L. Gratton (2008). Shaping Aviation Integrity - Two RAIMs for Safety. *GPS World*, Vol. 19, No. 4, pp. 42-49.

Wendel, J., T. Olbert and G.F. Trommer (2003). Enhancement of a tightly coupled GPS/INS system for high precision attitude determination of land vehicles. *Proc. of ION 57th annual meeting/CIGTF 22nd guidance test symposium*, Albuquerque, NM, 23-25 June 2003, pp. 200-208.